J|A|C|S ARTICLES

Published on Web 08/23/2010

Mapping Solvation Dynamics at the Function Site of Flavodoxin in Three Redox States

Chih-Wei Chang,¶ Ting-Fang He,¶ Lijun Guo, Jeffrey A. Stevens, Tanping Li, Lijuan Wang, and Dongping Zhong*

Departments of Physics, Chemistry, and Biochemistry, Programs of Biophysics, Chemical Physics, and Biochemistry, 191 West Woodruff Avenue, The Ohio State University, Columbus, Ohio 43210

Received June 9, 2010; E-mail: dongping@mps.ohio-state.edu

Abstract: Flavoproteins are unique redox coenzymes, and the dynamic solvation at their function sites is critical to the understanding of their electron-transfer properties. Here, we report our complete characterization of the function-site solvation of holoflavodoxin in three redox states and of the binding-site solvation of apoflavodoxin. Using intrinsic flavin cofactor and tryptophan residue as the local optical probes with two site-specific mutations, we observed distinct ultrafast solvation dynamics at the function site in the three states and at the related recognition site of the cofactor, ranging from a few to hundreds of picoseconds. The initial ultrafast motion in 1−2.6 ps reflects the local water-network relaxation around the shallow, solvent-exposed function site. The second relaxation in 20−40 ps results from the coupled local water−protein fluctuation. The third dynamics in hundreds of picoseconds is from the intrinsic fluctuation of the loose loops flanking the cofactor at the function site. These solvation dynamics with different amplitudes well correlate with the redox states from the oxidized form, to the more rigid semiquinone and to the much looser hydroquinone. This observation of the redox control of local protein conformation plasticity and water network flexibility is significant, and such an intimate relationship is essential to the biological function of interprotein electron transfer.

Introduction

Flavoproteins are ubiquitous in biology and have unique electron-transfer (ET) properties due to the rich redox chemistry of the cofactor flavin molecules.[1−7] They mostly contain flavin mononucleotide (FMN) and flavin adenine dinucleotide (FAD) as their cofactors and participate in a variety of biological functions such as cell apoptosis,[8] detoxification,[9] redox reactions,[7,10] light-driven DNA repair,[11,12] and blue-light photoreceptors.[11,13,14] To perform these various biological activities, the dynamical motions at function sites are essential to their catalytic reactions, as we have recently observed in photolyases.[12,15] Here, we choose an ET flavoprotein of flavodoxin as a model system and systematically characterize the function-site solvation in its three redox states of oxidized form (OX), one-electron reduced neutral semiquinone (SQ), and two-electron fully reduced anionic hydroquinone (HQ). Such characterization of the local solvation in the three states is critical to understanding how the functional ET dynamics are modulated by local protein motions in flavodoxin.

Flavodoxin is a small family of flavoproteins with FMN as the cofactor and has been recognized as the electron carrier in many bacteria.[16−18] The X-ray structures in three redox states have been solved[19] and Figure 1 (top left) shows the crystal structure of wild-type *Desulfovibrio vulgaris* flavodoxin in its oxidized state, which is constituted of a central five-stranded parallel β-sheet flanked by two α-helices. The FMN cofactor is bound with three loops at the top of the protein and is therefore solvent exposed. There are total 6 polar/charged amino acid residues (S58, T59, W60, D62, Y98, and C102) within 6 Å from the isoalloxazine ring of FMN, and FMN is sandwiched by two aromatic residues of W60 and Y98 (Figure 1, top middle). In the other two redox states, the X-ray structures show a significant cis−trans peptide bond conversion between G61

¶ These authors have made equal contributions.

(1) Walsh, C. *Acc. Chem. Res.* **1980**, *13*, 148–155.
(2) Bruice, T. C. *Acc. Chem. Res.* **1980**, *13*, 256–262.
(3) Ghisla, S.; Massey, V. *Eur. J. Biochem.* **1989**, *181*, 1–17.
(4) Fraaije, M. W.; Mattevi, A. *Trends Biochem. Sci.* **2000**, *25*, 126–132.
(5) Joosten, V.; van Berkel, W. J. H. *Curr. Opin. Chem. Biol.* **2007**, *11*, 195–202.
(6) Müller, F. In *Topics in Current Chemistry 108*; Boschke, F. L., Ed.; Springer: Berlin, 1983; pp 71−107.
(7) Müller, F., Ed. *Chemistry and Biochemistry of Flavoenzymes*; CRC Press: Boca Raton, FL, 1990−1991; Vols. I−III.
(8) Churbanova, I. Y.; Sevrioukova, I. F. *J. Biol. Chem.* **2008**, *283*, 5622–5631.
(9) Chen, H.; Hopper, S. L.; Cerniglia, C. E. *Microbiology* **2005**, *151*, 1433–1441.
(10) Massey, V. *Biochem. Soc. Trans.* **2000**, *28*, 283–296.
(11) Sancar, A. *Chem. Rev.* **2003**, *103*, 2203–2237.
(12) Kao, Y.-T.; Saxena, C.; Wang, L.; Sancar, A.; Zhong, D. *Proc. Natl. Acad. Sci. U.S.A.* **2005**, *102*, 16128–16132.
(13) Lin, C.; Shalitin, D. *Annu. Rev. Plant. Biol.* **2003**, *54*, 469–496.
(14) Cashmore, A. R.; Jarillo, J. A.; Wu, Y.; Liu, D. *Science* **1999**, *284*, 760–765.
(15) Chang, C.-W.; Kao, Y.-T.; Li, J.; Tan, C.; Li, T.; Saxena, C.; Liu, Z.; Wang, L.; Sancar, A.; Zhong, D. *Proc. Natl. Acad. Sci. U.S.A.* **2010**, *107*, 2914–2919.
(16) Simondsen, R. P.; Tollin, G. *Mol. Cell. Biochem.* **1980**, *33*, 13–24.
(17) Sancho, J. *Cell. Mol. Life Sci.* **2006**, *63*, 855–864.
(18) Setif, P. *Biochim. Biophys. Acta. Bioenerg.* **2001**, *1507*, 161–179.
(19) Watt, W.; Tulinsky, A.; Swenson, R. P.; Watenpaugh, K. D. *J. Mol. Biol.* **1991**, *218*, 195–208.

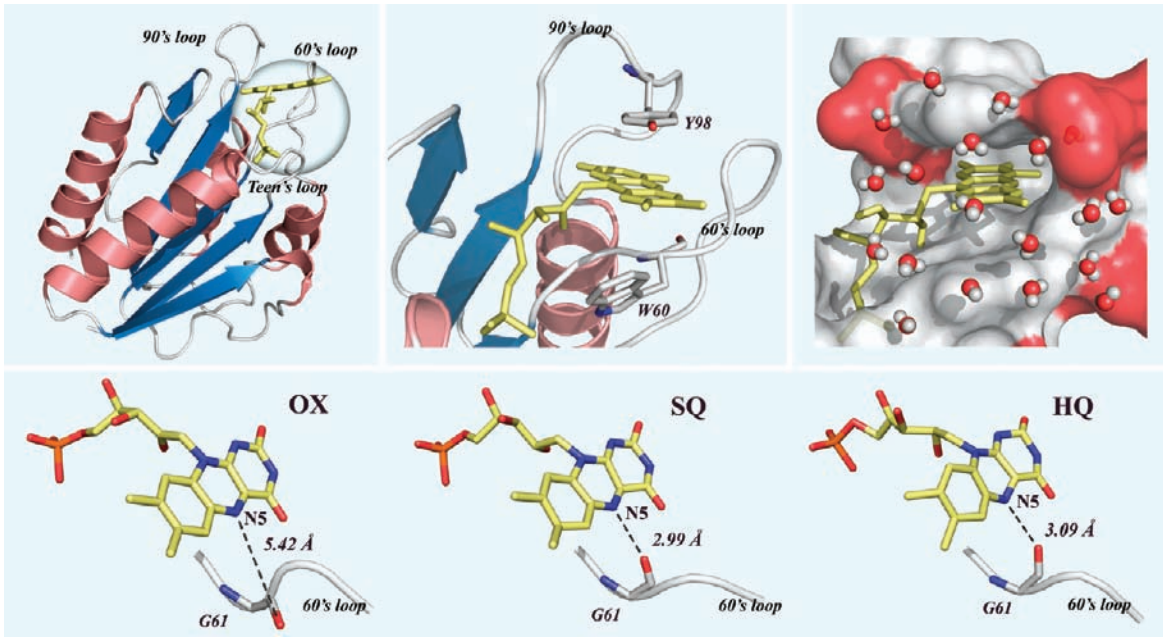

Figure 1. *Top panel:* (Left) X-ray crystal structure of oxidized *D. vulgaris* flavodoxin (PDB: 3FX2). (Middle) Close view of the FMN binding site embraced by two 60's and 90's loops. The FMN cofactor is sandwiched by two aromatic resides of W60 and Y98. (Right) Surface-map representation of a snapshot of 1-ns MD simulations, showing the function site with hydrating water molecules within 6 Å from the isoalloxazine ring and neighboring negatively charged residues (red). *Lower panel:* Local X-ray structures of three redox states show the loop flipping in SQ and HQ states to form a hydrogen bond with N5 of the isoalloxazine ring.

and D62, resulting in the formation of a hydrogen bond between the N5 hydrogen of the isoalloxazine ring and the carbonyl oxygen of G61 (Figure 1, bottom panel).[19] Figure 1 (top right) also shows a snapshot of our molecular dynamics (MD) simulations (1 ns) and clearly the FMN moiety is inserted into the hydrophobic pocket, and the exposed dimethylbenzene ring is surrounded by surface water molecules and neighboring negatively charged residues.

Using the intrinsic cofactor FMN as the local optical probe without extrinsic labeling, we are able to map out the entire evolution of local relaxations upon excitation at the function site in three redox states. To eliminate the potential ET quenching of excited FMN from the stacked aromatic residues of W60 and Y98 in OX and SQ states,[20−24] we have designed a double mutation of W60F/Y98F using the redox inert residue of phenylalanine and reported the excited-state FMN lifetimes in 6 ns, 230 ps, and 800 ps for the three redox states of OX, SQ, and HQ, respectively.[24] The long lifetime of 6 ns in the oxidized state provides a sufficient time window to measure various local motions.[15,25−27] By examining the femtosecond (fs)-resolved fluorescence dynamics and entire emission spectra of excited FMN at the function site, we observed the very different solvation dynamics in the three states and thus reveal their different local properties, structurally and dynamically, at the function site. We also examine the solvation dynamics of the FMN binding site in apoflavodoxin without FMN, using intrinsic W60 as a local optical probe by mutation of the other tryptophan residue (W140F). The single W60 gates the entrance of the binding pocket and thus also directly report the local water and protein motions at the binding site of apoflavodoxin.

Materials and Methods

Protein Preparation. The procedures of the expression and purification for *D. vulgaris* flavodoxin wild type and its mutants have been well established.[28] Upon purification the two flavodoxin mutants (W60F/Y98F and W140F) contained the oxidized FMN and was then converted to either the neutral radical semiquinone form[29] ($FMNH^{\bullet}$) or the two-electron reduced anionic hydroquinone state[30] ($FMNH^{-}$) under the anaerobic conditions. For fs-resolved experiments, the oxidized flavodoxin was prepared at the concentration of 50 μM in 50 mM phosphate buffer solution at pH 7. For the reduced states, the samples in 200−250 μM were mixed with the reducing agents in 50 mM MOPS buffer at pH 7 for the semiquinone and in 50 mM phosphate buffer at pH 8.3 for the hydroquinone. The FMN sample (USBioAnalyzed, more than 98% weight purity) was directly used without further purification with a concentration of 400 μM in 50 mM phosphate buffer at pH 7. Apoflavodoxin of the W140F mutant was prepared by following the well-documented trichloroacetic acid procedure[31] except that the buffer solution of 50 mM Tris-HCl at pH 7.5 at room temperature was used throughout the preparation.

Femtosecond Methods. All fs-resolved measurements were carried out using the fluorescence up-conversion method. The

(20) Mataga, N.; Chosrowjan, H.; Taniguchi, S.; Tanaka, F.; Kido, N.; Kitamura, M. *J. Phys. Chem. B* **2002**, *106*, 8917–8920.
(21) Zhong, D.; Zewail, A. H. *Proc. Natl. Acad. Sci. U.S.A.* **2001**, *98*, 11867–11872.
(22) Pan, J.; Byrdin, M.; Aubert, C.; Eker, A. P. M.; Brettel, K.; Vos, M. H. *J. Phys. Chem. B* **2004**, *108*, 10160–10167.
(23) Wang, H.; Saxena, C.; Quan, D.; Sancar, A.; Zhong, D. *J. Phys. Chem. B* **2005**, *109*, 1329–1333.
(24) Kao, Y.-T.; Saxena, C.; He, T.-F.; Guo, L.; Wang, L.; Sancar, A.; Zhong, D. *J. Am. Chem. Soc.* **2008**, *130*, 13132–13139.
(25) Zhong, D. *Adv. Chem. Phys.* **2009**, *143*, 83–149.
(26) Zhang, L.; Wang, L.; Kao, Y.-T.; Qiu, W.; Yang, Y.; Okobiah, O.; Zhong, D. *Proc. Natl. Acad. Sci. U.S.A.* **2007**, *104*, 18461–18466.
(27) Zhang, L.; Yang, Y.; Kao, Y.-T.; Wang, L.; Zhong, D. *J. Am. Chem. Soc.* **2009**, *131*, 10677–10691.
(28) Swenson, R. P.; Krey, G. D. *Biochemistry* **1994**, *33*, 8505–8514.
(29) Massey, V.; Stankovich, M.; Hemmerich, P. *Biochemistry* **1978**, *17*, 1–8.
(30) Mayhew, S. G. *Eur. J. Biochem.* **1978**, *85*, 535–547.
(31) Vervoort, J.; Heering, D.; Peelen, S.; van Berkel, W. *Methods in Enzymology 243*; Peck, H. D.; LeGall, J., Eds.; Academic Press: San Diego, 1994; pp 188−203.

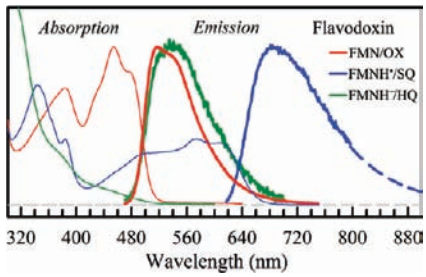

Figure 2. Steady-state absorption (thin line) and emission (thick line) spectra of W60F/Y98F mutant in OX, SQ, and HQ states. The excitation wavelengths were 400 nm for OX and HQ states, and 560 nm for SQ state. For SQ state, the emission spectrum at the red side was fitted with a log-normal function to extrapolate the emission longer than 800 nm as shown in the dashed line.

experimental layout has been described elsewhere.[32] Briefly, the pump wavelengths were set at 400 nm for holoflavodoxin in OX and HQ states and FMN in buffer solution, at 560 nm for holoflavodoxin in SQ state, and at 290 nm for apoflavodoxin. The pulse energy typically was attenuated to 50−100 nJ for the OX state, free FMN and apoflavodoxin, and to 140−200 nJ for SQ and HQ states. The instrument response time under the current noncollinear geometry is about 450 fs, and all data were taken at a magic angle (54.7°). The fs-resolved emission spectra at various delay times were obtained by scanning the mixing crystal angles and monochromator wavelengths simultaneously over the entire emission range. The time zero at each wavelength was carefully calibrated and a variety of delay times were appropriately chosen to reconstruct the three-dimensional fs-resolved emission spectra.

Results and Discussion

Ultrafast Fluorescence Transients and Solvation Dynamics in Three Redox States. Figure 2 shows the steady-state absorption and emission spectra of the W60F/Y98F mutant in different redox states. The absorption spectra in three redox states are similar to those of the wild type,[28] indicating that the mutant has a negligible structural perturbation and can represent wild-type flavodoxin. The corresponding weak emission spectra are shown in the thick lines. The steady-state fluorescence emission of OX state shows a peak at 515 nm with a shoulder at 545 nm while in SQ and HQ states the spectra have the significant broadening around the peak regions of 680 and 530 nm, respectively, leading to the nonlog-normal emission profiles. These structural features in emission typically result from the heterogeneous electrostatic distributions and different structural flexibility around the (partially) buried chromophore inside the protein.[15,33]

Panels A−C of Figure 3 show respectively several typical fluorescence transients of OX, SQ, and HQ states gated from the blue to red side of the emission spectra. As a comparison, we also measured the dynamics of FMN* in buffer solution (Figure 3D). All transients were taken within 3.5-ns time windows and exhibit a general trend of decay at the blue side and rise at the red side, a manifestation of typical solvation dynamics. Strikingly, the transients show significantly different decay behaviors for the three states. In OX state (Figure 3A), the transients at the blue side are fitted with three solvation components ranging from 0.9−1.8, 9−30, and 600−700 ps besides the long lifetime component in 6 ns. After the emission peak, the transients show rise components in 20−30 ps. In SQ state, the transients (Figure 3B) are clearly slower than those in OX state. At the blue side, the transients exhibit two decay components in 3.5−5 and 25−58 ps. Due to the short lifetime (230 ps) of SQ state, the second solvation component could mix with the lifetime emission, and any further slow relaxation will not be detected. Thus, the relaxation is not completed yet before the total excited-state deactivation. At the red side, the rise components in 1.4−5 ps are clearly present. In HQ state, the solvation dynamics at the blue side become faster again in 0.9−3.5, 10−31, and 55−300 ps, similar to those observed in OX state, but with much more pronounced amplitude for the first component. The third relaxation in hundreds of picoseconds could also mix with the lifetime component of 800 ps. At the red side, we also observed a fast decay component of 35 ps (10−15%) besides the lifetime decay (Figure 3C), indicating a loose binding pocket to allow $FMNH^-$ to proceed to a butterfly bending and distortion motions for fast deactivation as also observed in (6−4) photolyase,[15,34] photoreceptor cryptochrome[35] and chemical systems.[24] In all the three redox states, at the far-red side of the emission, the transients become fast decay again, a general phenomenon for the slow solvation in heterogeneous protein environments through various spectral tunings.[15,36]

To extract the solvation correlation function, the fs-resolved emission spectra (FRES) are typically constructed using the obtained transients at various wavelengths.[37,38] However, for the irregular spectral profiles not following the standard log-normal distribution, we have to directly measure the FRES to follow the entire spectral evolution. Instead of using the emission peaks, we calculated the averaged frequency ($\bar{\nu}$) of FRES to obtain the averaged Stokes shifts and thus derive the solvation correlation function.[39]

Femtosecond-Resolved Emission Spectra and Redox-Dependent Correlation Functions. Figure 4 shows the reconstructed three-dimensional plots of FRES (upper panel) and a few snapshots at various delay times (lower panel) in the three states. The corresponding steady-state emission spectra are shown at the bottom. In all cases, we observed minor spectral shifts but obvious emission profile changes. As we observed in photolyases,[15] the spectra of FMN in the three states here show little shifts of the emission peaks but obvious shrinking at the blue side and broadening at the red side. Such shape changes by the spectral tuning reflect heterogeneous local electrostatics and corresponding anisotropic relaxation.[15,40] To quantify such changes of local relaxations, we calculated the averaged frequencies and used the relative stabilization energies $\Delta E(t)$, relative to the time-zero averaged energy, to represent the solvation dynamics. The derived functions then

(32) Saxena, C.; Sancar, A.; Zhong, D. *J. Phys. Chem. B* **2004**, *108*, 18026–18033.
(33) Shi, X.; Abbyad, P.; Shu, X.; Kallio, K.; Kanchanawong, P.; Childs, W.; Remington, S. J.; Boxer, S. G. *Biochemistry* **2007**, *46*, 12014–12025.
(34) Li, J.; Liu, Z.; Tan, C.; Guo, X.; Wang, L.; Sancar, A.; Zhong, D. *Nature* **2010**, *466*, 887−890.
(35) Kao, Y.-T.; Tan, C.; Song, S.; Ozturk, N.; Li, J.; Wang, L.; Sancar, A.; Zhong, D. *J. Am. Chem. Soc.* **2008**, *130*, 7695–7701.
(36) Zhang, L.; Kao, Y.-T.; Qiu, W.; Wang, L.; Zhong, D. *J. Phys. Chem. B* **2006**, *110*, 18097–18103.
(37) Horng, M. L.; Gardecki, J. A.; Papazyan, A.; Maroncelli, M. *J. Phys. Chem.* **1995**, *99*, 17311–17337.
(38) Lu, W.; Kim, J.; Qiu, W.; Zhong, D. *Chem. Phys. Lett.* **2004**, *388*, 120–126.
(39) Maroncelli, M.; Fleming, G. R. *J. Chem. Phys.* **1987**, *86*, 6221–6239.
(40) Philip, A. F.; Nome, R. A.; Papadantonakis, G. A.; Scherer, N. F.; Hoff, W. D. *Proc. Natl. Acad. Sci. U.S.A.* **2010**, *107*, 5821–5826.

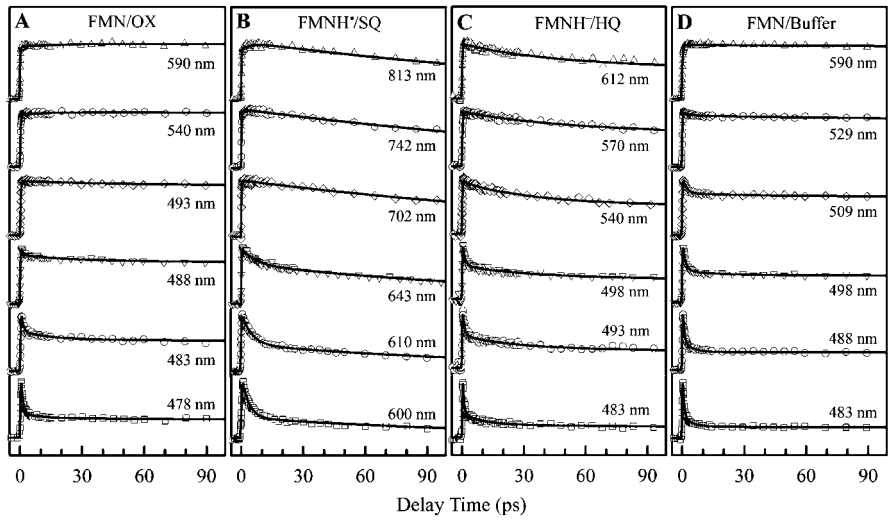

Figure 3. Normalized femtosecond-resolved fluorescence transients of W60F/Y98F mutant in (A) OX, (B) SQ, (C) HQ states, and (D) FMN in buffer solution. These transients were gated from the blue to red side of the emission spectra. Note the drastic differences in three redox states.

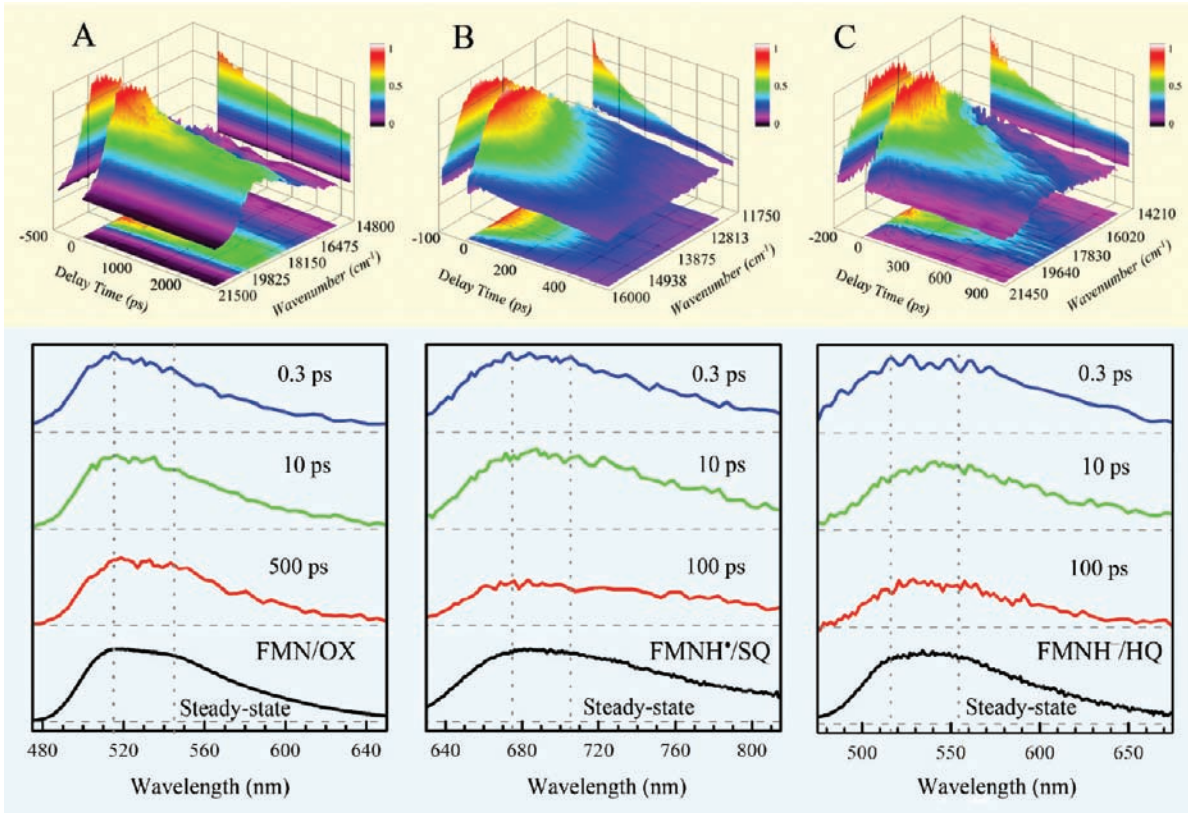

Figure 4. *Upper panel*: Three-dimensional representation of femtosecond-resolved emission spectra of W60F/Y98F mutant in (A) OX, (B) SQ, and (C) HQ states. The intensity is scaled by a color code. *Lower panel*: Three snapshots of the femtosecond-resolved emission spectra at typical delay times for the three states with their corresponding steady-state emission spectra. For comparison and clarity, the steady-state emission peaks are indicated by gray dotted lines.

could be fitted by the following equation with three exponential decays.

$$\Delta E = \Delta E_1\, e^{-t/\tau_1} + \Delta E_2\, e^{-t/\tau_2} + \Delta E_3\, e^{-t/\tau_3} + \Delta E_\infty, \quad \Delta E_1 + \Delta E_2 + \Delta E_3 + \Delta E_\infty = 0 \quad (1)$$

To further evaluate the local flexibility through solvation, we define an averaged solvation speed (or averaged environment reorganization rate) in terms of energy drop (in cm^{-1}) per picosecond by local relaxation.[15,27]

$$S_1 = \frac{\Delta E_1}{\tau_1},\ S_2 = \frac{\Delta E_2}{\tau_2},\ S_3 = \frac{\Delta E_3}{\tau_3} \quad (2)$$

Figure 5 shows the derived relaxation functions in the three states, and Table 1 gives the summary of their time scales,

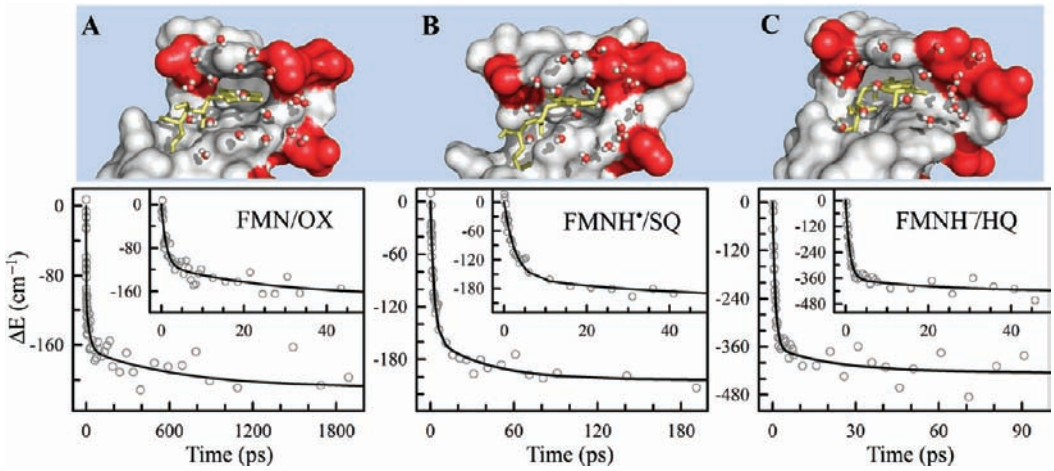

Figure 5. *Upper panel:* Surface-map representation of a snapshot of the function site of flavodoxin in (A) OX, (B) SQ, and (C) HQ states from 1-ns MD simulations. Only water molecules within 6 Å from the isoalloxazine ring are shown. The negatively charged residues are indicated in red. *Lower panel*: Solvation responses at the function site of flavodoxin in three redox states represented by the stabilization energy changes (ΔE) with time. The insets show the responses at short time scale.

Table 1. Results of Solvation Dynamics at the Function Site of Flavodoxin in Three Redox States[a]

environment	probe	τ_1	ΔE_1	τ_2	ΔE_2	τ_3	ΔE_3	S_1	S_2	S_3	ΔE_T
flavodoxin (W60F/Y98F)	FMN/OX	1	111	25	54	670	44	111	2.16	0.07	209
	$FMNH^•$/SQ	2.6	154	40	50			59	1.25		204
	$FMNH^-$/HQ	1	360	21	59	180	11	360	2.8	0.06	430
flavodoxin (wt)	$FMNH^-$/HQ	0.9	345	26	97	81	6	383	3.7	0.07	448
buffer solution[b]	FMN	0.4	45	1.4	296	11	80				421
apoflavodoxin (W140F)[c]	W60	1.1	594	18.3	586			540	32		1180

[a] The solvation dynamics were derived by calculating the averaged frequency changes with time. The time constant (τ), total stabilization energy ($\Delta E_T = \Delta E_1 + \Delta E_2 + \Delta E_3$) and solvation speed ($S$) are in units of ps, cm^{-1}, and cm^{-1}/ps, respectively. [b] The solvation dynamics derived from the peak shifts by the log-normal fitting are $\tau_1 = 0.4$ ps (121 cm^{-1}), $\tau_2 = 1.4$ ps (400 cm^{-1}), and $\tau_3 = 11$ ps (133 cm^{-1}). [c] The solvation dynamics derived from the peak shifts by the log-normal fitting are $\tau_1 = 1.1$ ps (595 cm^{-1}) and $\tau_2 = 18.4$ ps (610 cm^{-1}).

stabilization energies, and solvation speeds. Clearly, the correlation functions of three redox states are significantly different.

Specifically, in OX state, the solvation dynamics occur in 1 (53%), 25 (26%), and 670 ps (21%) (Figure 5A). For the shallow binding pocket with the partial exposure of FMN to the protein surface, the three time scales mainly represent the local water-network relaxation, coupled water−protein fluctuation, and intrinsic collective protein motion, respectively.[25−27,41,42] From our MD simulations, about 20−25 water molecules are found within 6 Å to the isoalloxazine ring of FMN and around the entrance of the function site (Figure 5A). Given the loop nature of the function site, the time scales of 1 and 25 ps are consistent with the dynamics of hydrating water molecules at the protein surface observed in the other proteins.[26,43] In SQ state, the solvation drastically slows down in 2.6 (75%) and 40 ps (25%) (Figure 5B). The MD simulations show no obvious changes in number of neighboring water molecules (Figure 5B), and the main difference is the local structures in the two redox states (Figure 1). The SQ protein has superior stability[44] and a tighter binding pocket due to the formation of a specific hydrogen bond between the N5 position of FMN and the backbone carbonyl oxygen of G61 (Figure 1), indicating a more rigid local structure (Figure 5B). Thus, such a structural change in rigidity directly affects the neighboring water-network flexibility and coupled water−protein fluctuations, leading to the observed slow solvation dynamics. The lack of observation of the third longtime protein relaxation in subnanoseconds is due to the short chromophore's lifetime (230 ps).

For HQ state, the solvation becomes faster again and the time scales are 1 (83%), 21 (14%), and 180 ps (3%), comparable to those of OX state, but with a significant increase of the first fast component (Figure 5C). From the X-ray structure,[19] our MD simulations (Figure 5C), and the NMR studies,[45] the shallow binding pocket become looser, mainly in the regions of 56−82 residues of the 60's loop and 91−103 residues of the 90's loop and largely due to the repulsion between $FMNH^-$ and the surrounding negatively charged residues such as D62 and D95 (Figure 1 and Figure 5C). Thus, the local hydrogen-bond network becomes more flexible, and also more water molecules can penetrate into or are trapped around the function site, resulting in a larger stabilization energy in 1 ps and suggesting a more polar environment in HQ state. Since the stabilization energy depends on the local polarization and the dipole-moment change ($\Delta\vec{\mu}$) between the ground and excited states and the recent experiments by Stark spectroscopy suggested a similar value of dipole-moment changes in three redox states,[46−48] the observed large increase of ΔE_1 (360 cm^{-1}) in

(41) Qiu, W.; Kao, Y.-T.; Zhang, L.; Yang, Y.; Wang, L.; Stites, W. E.; Zhong, D.; Zewail, A. H. *Proc. Natl. Acad. Sci. U.S.A.* **2006**, *103*, 13979–13984.
(42) Li, T.; Hassanali, A. A.; Kao, Y.-T.; Zhong, D.; Singer, S. J. *J. Am. Chem. Soc.* **2007**, *129*, 3376–3382.
(43) Qiu, W.; Wang, L.; Lu, W.; Boechler, A.; Sanders, D. A. R.; Zhong, D. *Proc. Natl. Acad. Sci. U.S.A.* **2007**, *104*, 5366–5371.
(44) Mayhew, S. G.; Foust, G. P.; Massey, V. *J. Biol. Chem.* **1969**, *244*, 803–810.
(45) Hrovat, A.; Blumel, M.; Lohr, F.; Mayhew, S. G.; Ruterjans, H. *J. Biomol. NMR* **1997**, *10*, 53–62.
(46) Salim, M.; Siddiqui, U.; Kodali, G.; Stanley, R. J. *J. Phys. Chem. B* **2008**, *112*, 119–126.
(47) Stanley, R. J.; Jang, H. *J. Phys. Chem. A* **1999**, *103*, 8976–8984.

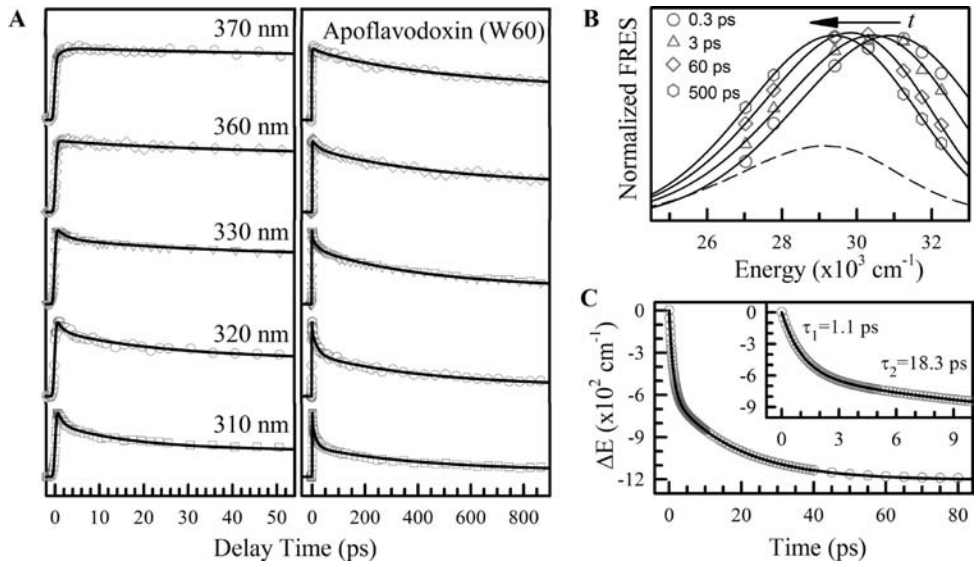

Figure 6. (A) Normalized femtosecond-resolved fluorescence transients of apoflavodoxin (W60) gated from the blue to the red side of the emission spectrum. The transients are shown at two different time scales. (B) Representative of normalized femtosecond-resolved emission spectra (FRES) at different delay times. The symbols represent the experimental data, and the solid lines are from the log-normal fitting. The dashed line is the steady-state emission spectrum. (C) Solvation response at the binding site of apoflavodoxin represented by the stabilization energy change (ΔE) with time, and the inset shows the short time range.

HQ state must reflect the local environment change and in this case both the local water network and protein structure probably become more flexible. Interestingly, we observed a very similar stabilization energy of ΔE_2 (50−60 cm^{-1}) for all the three states, reflecting the same amount of relaxation energy from coupled water−protein fluctuations. Since there is no ET quenching of $FMNH^{-*}$ in HQ state, we also examined the solvation dynamics of the wild-type protein and obtained results similar to those of the mutant (Table 1). The increase in stabilization energy of ΔE_2 (97 cm^{-1}) probably results from the contributions of stacked Y98 (polar) and W60 residues, whereas in the mutant, FMN is sandwiched by the nonpolar residue of phenylalanine. The observed small ΔE_3 and fast τ_3 are due to the short lifetime of the wild-type protein (300 ps).

The solvation speeds in the three states (Table 1) are dramatically different and directly elucidate the local flexibility. The first and second solvation speeds (S_1 and S_2) systematically change from the largest in HQ state, to the middle in OX state, and to the smallest in SQ, reflecting an evolution of the hydrogen-bond network from flexible to rigid and correlating well with the local protein mobility. The third solvation speed (S_3) is similar, indicating an intrinsic collective motion of flavodoxin. Thus, we observed a relatively tight function site in SQ state with both rigid local water networks and inflexible side chains and a relatively loose function site in HQ state with considerable water-network flexibility and side-chain mobility, a drastic difference of the local properties for these two physiological *in vivo* states in cell.

We also examined the solvation dynamics of FMN in buffer solution as a control to quantify the stabilization energy (Table 1). We observed three time scales of 0.4 (11%), 1.4 (70%), and 11 ps (19%). Compared to bulk water,[38,49] the solvation dynamics overall slow down, presumably resulting from the more hydrogen-bond networks and ions of the ribityl phosphate moiety. For the log-normal distribution of FRES, the relaxation energy can be derived by calculating either the emission peak shifts or averaged frequency changes (Table 1). We obtained a stabilization energy of 341 cm^{-1} for the first two fast relaxations, similar to the values (345−360 cm^{-1}) in HQ state but much larger than those in OX and SQ states (111−154 cm^{-1}), suggesting more and looser water molecules in the function site of HQ state, less mobile water molecules in OX state, and even more rigid in SQ state.

Binding Site Solvation and Protein Surface Hydration. We further examined the local solvation dynamics at the binding site without the cofactor FMN inside the pocket. The X-ray structure of apoflavodoxin[50] shows that the tryptophan residue W60 slightly rotates and perfectly covers the entrance of the binding pocket and lies down at the protein surface with a maximum emission peak at 343 nm. Using the mutant W140F, the single tryptophan W60 can be used as a local probe to study the surface hydration dynamics around the binding site as was extensively used in our other studies.[25] Figure 6 shows the final results, and the obtained time scales and stabilization energies are also given in Table 1. Significantly, we observed the two similar relaxations in 1 (50%) and 18.3 ps (50%), reflecting the initial local water-network relaxations and subsequent water−protein coupling fluctuations, completely consistent with the dynamics observed in the other proteins with similar local protein properties.[26,43] The lack of the possible third relaxation is due to mixing with one short lifetime (400 ps) of W60. Compared with holoflavodoxin in OX state, the second relaxation (18.3 ps) of the water−protein coupling motion becomes obviously faster, reflecting a more flexible structure in apoflavodoxin and a more rigid binding structure in holoflavodoxin. The observed greater stabilization energy by a factor of 4−5 results from the larger change of dipole moments ($\Delta\vec{\mu}$) of W60,

(48) Stanley, R. J.; Siddiqui, M. S. *J. Phys. Chem. A* **2001**, *105*, 11001–11008.
(49) Jimenez, R.; Fleming, G. R.; Kumar, P. V.; Maroncelli, M. *Nature* **1994**, *369*, 471–473.
(50) Genzor, C. G.; PeralesAlcon, A.; Sancho, J.; Romero, A. *Nat. Struct. Biol.* **1996**, *3*, 329–332.

consistent with the reported values of dipole-moment changes, 1.1 D for FMN[46] and ~5 D for tryptophan.[51] Thus, for the shallow and hydrophobic binding site of FMN, the local hydration dynamics probed by W60 show the fast water-network relaxations, similar both in time and energy to those of the function-site solvation probed by the cofactor FMN. Moreover, the two probes can distinguish the different water−protein coupling motions, reflecting the intrinsic different flexibility of the local structures with and without binding of the cofactor FMN.

Conclusion

We reported a systematic study of the local solvation dynamics in the binding site of apoflavodoxin and in the function site of holoflavodoxin in three redox states using the intrinsic tryptophan (W60) and cofactor FMN as the local optical probes without extrinsic labeling. With site-directed mutations, we designed two mutants to reach the specificity for W60 and to eliminate the potential quenching of FMN, respectively. With femtosecond resolution, we observed the distinct solvation dynamics in apoflavodoxin and in three redox states of holoflavodoxin. From the apoflavodoxin to oxidized holoflavodoxin (FMN), we observed similar fast water-network relaxations in 1 ps but different water−protein coupling fluctuations (18.3 vs 25 ps) from the two different structural flexibilities. From the oxidized to semiquinone ($FMNH^{\bullet}$) states, the local structure becomes more rigid due to the extra hydrogen-bond formation by the redox switching. The local solvation dynamics significantly slow down to 2.6 and 40 ps, a clear correlation between the local structural rigidity and water-network immobility. From the semiquinone to hydroquinone ($FMNH^{-}$) states, the solvation relaxations become faster again in 1 and 21 ps with a significant increase in total solvation energy, due to a more polar environment with more mobile water molecules in a looser and larger pocket caused by the negative repulsion between the anionic cofactor and neighboring negatively charged residues. With the long excited-state lifetime of the local probe, we also observed the intrinsic protein relaxation in hundreds of picoseconds as shown in oxidized and partially hydroquinone states.

The observed distinct solvation dynamics in three redox states are significant, reflecting the redox dependence of protein conformation plasticity and water network flexibility, ultimately relating to the biological functions. As an electron shuttle, the compact, immobile function site in the semiquinone state is ideal to dock into electron-donor partners (such as flavodoxin reductase or photosystem I) for reduction, and the loose, flexible function site in the hydroquinone state is necessary to deliver electrons to a variety of electron-acceptor partners (such as ferreodoxin-$NADP^{+}$ reductase or methionine synthase) with nonspecific interacting interfaces.[18,52−54] The observed correlation between the redox states and the solvation dynamics is fundamental and elucidates the intrinsic dynamical relationship between hydration networks and local protein structures. For a given redox state with a unique structure, it requires a certain water network for its stability and flexibility. In turn, the dynamics of such a specific water network controls the flexibility of the local protein structure, an intimate relationship of water−protein coupling motions. Clearly, such a relationship of redox states with protein conformation flexibility and water network mobility at the function site is essential for performing the various biological activities.

Synopsis

Mapping the solvation dynamics at the function site of flavodoxin at three redox states using the FMN cofactor as the local optical probe. The observed distinct dynamics are well correlated with three redox states and active-site flexibility, relating to the final intermolecular electron transfer properties.

Acknowledgment. We thank Prof. Richard P. Swenson for the generous gift of the flavodoxin plasmid. We also thank Donghui Quan for the initial experiment shown in Figure 6. The work is supported in part by the National Institute of Health (GM074854), the National Science Foundation (CHE-0748358), the Packard fellowship, and the Sloan fellowship.

JA1050154

(51) Pierce, D. W.; Boxer, S. G. *Biophys. J.* **1995**, *68*, 1583–1591.

(52) Hall, D. A.; Kooi, C. W. V.; Stasik, C. N.; Stevens, S. Y.; Zuiderweg, E. R. P.; Matthews, R. G. *Proc. Natl. Acad. Sci. U.S.A.* **2001**, *98*, 9521–9526.

(53) Goni, G.; Herguedas, B.; Hervas, M.; Peregrina, J. R.; De la Rosa, M. A.; Gomez-Moreno, C.; Navarro, J. A.; Hermoso, J. A.; Martinez-Julvez, M.; Medina, M. *Biochim. Biophys. Acta. Bioenerg.* **2009**, *1787*, 144–154.

(54) Frago, S.; Lans, I.; Navarro, J. A.; Hervas, M.; Edmondson, D. E.; De la Rosa, M. A.; Gomez-Moreno, C.; Mayhew, S. G.; Medina, M. *Biochim. Biophys. Acta. Bioenerg.* **2010**, *1797*, 262–271.